

Thermodynamic Properties of Model Solids with Short-ranged Potentials from Monte Carlo Simulations and Perturbation Theory

A. Díez

Departamento de Física Aplicada, Universidad de Cantabria, E-39005 Santander, Spain

J. Largo

Dipartimento di Fisica, Università di Roma La Sapienza, I-00185 Roma, Italy

J. R. Solana*

Departamento de Física Aplicada, Universidad de Cantabria, E-39005 Santander, Spain

(Dated: October 11, 2018)

Abstract

Monte Carlo simulations have been performed to determine the excess energy and the equation of state of fcc solids with Sutherland potentials for wide ranges of temperatures, densities and effective potential ranges. The same quantities have been determined within a perturbative scheme by means of two procedures: i) Monte Carlo simulations performed on the reference hard-sphere system and ii) second order Barker-Henderson perturbation theory. The aim was twofold: on the one hand, to test the capability of the 'exact' MC-perturbation theory of reproducing the direct MC simulations and, on the other hand, the reliability of the Barker-Henderson perturbation theory, as compared with direct MC simulations and MC-perturbation theory, to determine the thermodynamic properties of these solids depending on temperature, density and potential range. We have found that the simulation data for the excess energy obtained from the two procedures are in close agreement with each other. For the equation of state, the results from the MC-perturbation procedure also agree well with direct MC simulations except for very low temperatures and extremely short-ranged potentials. Regarding the Barker-Henderson perturbation theory, we have found that, surprisingly, the first-order approximation is in closer agreement with simulations than the second-order one.

PACS numbers: 05.10.Ln, 05.70.Ce, 64.10.+h

I. INTRODUCTION

The Sutherland potential is of the form

$$u(r) = \begin{cases} \infty, & r \leq \sigma \\ -\epsilon \left(\frac{\sigma}{r}\right)^\gamma, & r > \sigma \end{cases} \quad (1)$$

where parameters σ and $-\epsilon$ account for diameter of the particles and the maximum potential depth, respectively, and the exponent γ determines the effective range of the potential, so that the higher is the value of γ the shorter is the effective range.

The shape of the potential function (1) resembles the shape of other widely used potentials, such as the Lennard-Jones potential, for $\gamma = 6$, the Girifalco potential for C_{60} , for $\gamma \approx 12$,¹ and the Mie potential, widely used to describe pure fluids and solutions as well as solids, for a wide range of values of γ depending on the real system to be modelled.² The advantage of a potential of the form (1) with respect to these others is that in the former the diameter of the particles is well defined. The simple mathematical form of the potential (1), together with its flexibility to reproduce a wide variety of intermolecular interactions, has led recently to a number of applications for modelling interactions in complex fluids^{3,4} and nanocomposite materials.⁵

In this situation, one might reasonably expect this kind of systems would have been extensively studied both from theory and from computer simulation. However, computer simulations on this system have been scarcely reported. For the fluid, quite extensive simulation data for the excess energy and the compressibility factor have been reported in ref.⁶ and more recently in⁷ for several values of γ and a wide range of densities and temperatures, particularly in the latter reference. Simulation data on the radial distribution function for the high density fluid may be found in ref.⁸ for several temperatures and effective ranges. Simulation data for liquid-vapour coexistence densities and critical parameters for several values of γ were reported in ref.⁹ and triple point parameters in ref.¹⁰.

Regarding theory, the amount of research devoted to this kind of fluids is equally scarce^{7,8,11,12,13}, although recently we reported⁷ a quite complete analysis of the performance of the Barker-Henderson perturbation theory^{14,15} for the thermodynamic properties of this kind of fluids, and still more recently⁸ we performed a similar analysis using the first-order mean spherical approximation.^{16,17}

In contrast with fluids, crystalline solids interacting by means of model potentials have been much less frequently studied, with the possible exception of the hard-sphere solid, and to the best of our knowledge the behaviour of solids with Sutherland potentials has not been studied before from theory nor computer simulation. This is the aim of this paper, for which we have performed extensive computer simulations for the thermodynamic properties of Sutherland fcc solids for several values of γ , temperatures and densities. These are described in the next Section. Section III, summarizes the foundations of two versions of the perturbation theory 1) an 'exact' first-order perturbation theory based on simulations performed on the reference hard-sphere fcc solid and the Barker-Henderson perturbation theory. These two theories are compared in Section IV with each other and with the simulation data reported in Section II, and the concluding remarks are presented in the same Section.

II. MONTE CARLO SIMULATIONS FOR FCC SOLIDS WITH SUTHERLAND POTENTIALS

We have performed NVT Monte Carlo simulations for fcc solids with potentials of the form (1) with $\gamma = 6, 12, 18$, and 36 , reduced temperatures $T^* = 0.6, 0.8, 1.0, 1.5, 2.0$ and 3.0 , and reduced densities ρ^* in the range $0.90 - 1.30$ with step 0.05 this covering most of the density range for the solid and some of the high density fluid. The potential cut-off distance was fixed at $r_c = 3\sigma$. Most of the systems consisted in $N = 500$ particles but some simulations were carried out with 2048 particles to test the influence of the size of the system. The particles were placed in a cubic box with periodic boundary conditions in a fcc configuration. The system was equilibrated for 2×10^4 cycles, each cycle consisting of an attempted move per particle and then the thermodynamic and structural properties were measured over the next 5×10^4 cycles, with partial averages every 500 cycles from which the statistical errors were determined as the standard deviation. Acceptance ratio was fixed at around 50% . The excess energy U^E was determined from the energy equation in the form

$$\frac{U^E}{N} = 2\pi\rho \int_0^\infty g(r)r^2u(r)dr \quad (2)$$

The compressibility factor Z was determined from the expression

$$Z = \frac{pV}{Nk_B T} = 1 + \frac{2}{3}\pi\rho\sigma^3 g(\sigma) + \frac{\gamma}{3}\epsilon \frac{U^E}{Nk_B T} \quad (3)$$

which results from the combination of eq. (2) with the virial theorem for the Sutherland potential.

Results are listed in Tables I-IV, in which corrections to account for the effect of the truncation of the potential have not been included. For the Sutherland potential with cut-off distance $r_c = 3\sigma$, the corrections for the compressibility factor and the excess energy are

$$\Delta Z = \frac{2}{3}\pi\gamma \frac{3^{3-\gamma}}{3-\gamma} \frac{\rho^*}{T^*} \quad (4)$$

and

$$\frac{\Delta U^E}{N\epsilon} = 2\pi \frac{3^{3-\gamma}}{3-\gamma} \rho^* \quad (5)$$

respectively.

III. PERTURBATION THEORY

In perturbation theories, the intermolecular potential is split in the form

$$u(r) = u_0(r) + u_1(r), \quad (6)$$

where $u_0(r)$ and $u_1(r)$ accounts essentially for the short-range and long-range contributions, respectively. The former is mainly due to the repulsive forces and the latter to the attractive ones. For the Sutherland potential (1), the obvious choice for these contributions is

$$u_0(r) = \begin{cases} \infty, & r \leq \sigma \\ 0, & r > \sigma \end{cases}, \quad (7)$$

and

$$u_1(r) = \begin{cases} 0 & r \leq \sigma \\ -\epsilon \left(\frac{\sigma}{r}\right)^\gamma, & r > \sigma \end{cases}, \quad (8)$$

respectively. Note that (7) is the hard sphere (HS) potential.

At high densities the thermodynamic and structural properties of a system are determined mainly by the first of these contributions, whence arise perturbation theories. These theories consider that the properties of the system at high densities are given by those of a reference system, one consisting of particles interacting by means of the potential $u_0(r)$ and providing the main contribution, plus a minor contribution due to $u_1(r)$ and considered as a perturbation of the former. As most of the thermodynamic systems with spherically-symmetric potentials at high temperatures behave much like a hard-sphere system, the latter is the obvious choice for the reference system. Therefore, it is natural to express the thermodynamic properties as a series expansion in terms of $1/T^*$, the inverse of the reduced temperature, with the zero-order term corresponding to the contribution of the reference system and the remaining terms accounting for the contribution of the perturbation. In this situation, the Helmholtz free energy, the radial distribution function, the excess energy, and the compressibility factor can be expressed in the form

$$\frac{F}{Nk_B T} = \sum_{n=0}^{\infty} \frac{F_n}{Nk_B T} \frac{1}{T^{*n}}. \quad (9)$$

$$g(r) = \sum_{n=0}^{\infty} g_n(r) \frac{1}{T^{*n}}, \quad (10)$$

$$\frac{U^E}{N\epsilon} = \sum_{n=0}^{\infty} \frac{U_n}{N\epsilon} \frac{1}{T^{*n}}, \quad (11)$$

$$Z = \sum_{n=0}^{\infty} Z_n \frac{1}{T^{*n}}, \quad (12)$$

where subscripts '0' correspond to the contributions due to the reference system which, for systems with the Sutherland potential, is the hard-sphere system.

A. 'Exact' First-order Perturbation Theory

Before analysing the performance of the Barker-Henderson perturbation theory for Sutherland solids, it is worth analysing the capability of an 'exact' perturbation theory for obtaining the thermodynamic properties of these solids. By 'exact' by mean a perturbation theory with the terms in expansions (10)-(12) obtained from computer simulations performed on the hard-sphere reference system, thus avoiding any theoretical approximation.

The procedure to determine the zero- and first-order terms in the expansion (10) by means of computer simulation was developed by Smith et al.¹⁸ quite a long time ago. They found

$$g_0(r_i + \Delta r/2) = \frac{3\langle N_i \rangle_0}{2\pi N \rho (r_{i+1}^3 - r_i^3)} \quad (13)$$

and

$$g_1(r_i + \Delta r/2) = -\frac{3 \sum_j \{ \langle N_i N_j \rangle_0 - \langle N_i \rangle_0 \langle N_j \rangle_0 \} u_1^*(r_j)}{2\pi N \rho (r_{i+1}^3 - r_i^3)} \quad (14)$$

In the preceding expressions N_i is the number of intermolecular distances in the range (r_i, r_{i+1}) , with $\Delta r = r_{i+1} - r_i \ll \sigma$ $i = 0, 1, \dots$, angular brackets mean an average, subscript 0 mean that the averages are performed in the reference HS system, and $u_1^*(r) = u_1(r)/\epsilon$.

Introducing the r.d.f. (10), truncated at first order, into the energy equation (2) provides the first- and second-order contributions to the excess energy in the form

$$U_1 = 2N\pi\rho \sum_i g_0(r_i) r_i^2 u_1(r_i) \Delta r \quad (15)$$

and

$$U_2 = 2N\pi\rho \sum_i g_1(r_i) r_i^2 u_1(r_i) \Delta r \quad (16)$$

respectively.

Introducing in turn the excess energy (11), truncated at first order, into the virial equation of state (3), provides the zero- and first-order contributions to the compressibility factor. They are

$$Z_0 = 1 + \frac{2}{3}\pi\rho\sigma^3 g_0(\sigma) \quad (17)$$

and

$$Z_1 = \frac{2}{3}\pi\rho\sigma^3 g_1(\sigma) + \frac{\gamma}{3}\epsilon \frac{U_1}{Nk_B T} \quad (18)$$

respectively.

In principle, the procedure could be generalised to obtain higher-order terms, but the computational effort increases with the order of the perturbative term and becomes impractical.

This procedure, that has been denoted Monte Carlo perturbation theory (MC-P),²¹ was applied to obtain the first terms in the perturbative expansions (10)-(12) for square-well fluids, first by Smith et al.¹⁸ and more recently by two of us.^{19,20,21} Very recently we have used successfully the same procedure to obtain the thermodynamic and structural properties of fluids with Sutherland potential.⁷ To the best of our knowledge, the procedures has never been applied to crystalline solids.

The explicit expressions of eqs. (10)-(12), truncated at the above-mentioned level, are as follows

$$g(x) = g_0(x) + g_1(x) \frac{1}{T^*} \quad (19)$$

where $x = r/\sigma$ is the reduced distance,

$$\frac{U^E}{N\epsilon} = \frac{U_1}{N\epsilon} + \frac{U_2}{N\epsilon} \frac{1}{T^*} \quad (20)$$

and

$$Z = Z_0 + \frac{1}{T^*} Z_1 \quad (21)$$

We have performed Monte Carlo simulations in the NVT ensemble of the reference HS fluid to obtain the perturbative terms in expressions (19)-(21). To this end, we considered a system consisting in 500 hard spheres in an placed in a fcc configuration within a cubic box with periodic boundary conditions. At each density, the system was allowed to equilibrate for 5×10^4 cycles and the averages involved in expressions (13) and (14) were calculated from the next 10^6 cycles. We chose $\Delta r = 0.005$ and the acceptance ratio was settled to about 50%. From these data, we have calculated the values of $g_0(x)$ and $g_1(x)$ from eqs. (13) and (14), respectively, and subsequently U_1 , U_2 , Z_0 , and Z_1 from eqs. (15)-(18).

B. Barker-Henderson perturbation theory

The Barker-Henderson perturbation theory (BH)^{14,15} provides expressions for the first- and second-order terms in the expansion (9). The first-order term is given by

$$\frac{F_1}{Nk_B T} = 2\pi\rho \int_0^\infty u_1^*(r)g_0(r)r^2 dr \quad (22)$$

The second-order term in the *macroscopic compressibility approximation* (mc) is

$$\frac{F_2}{Nk_B T} = -\pi\rho k_B T \int_0^\infty [u_1^*(r)]^2 \left(\frac{\partial \rho}{\partial p} \right)_0 g_0(r)r^2 dr \quad (23)$$

and in the *local compressibility approximation* (lc)

$$\frac{F_2}{Nk_B T} = -\pi\rho k_B T \int_0^\infty [u_1^*(r)]^2 \left(\frac{\partial [\rho g_0(r)]}{\partial p} \right)_0 r^2 dr \quad (24)$$

The corresponding contributions to the excess energy can be readily obtained from the thermodynamic relationship

$$\frac{U^E}{N\epsilon} = -T^{*2} \left[\frac{\partial (F/Nk_B T)}{\partial T^*} \right]_V \quad (25)$$

and those for the compressibility factor from

$$Z_n = \frac{p_n V}{Nk_B T} = \rho \left[\frac{\partial (F_n/Nk_B T)}{\partial \rho} \right]_T \quad (26)$$

Using suitable expressions for the r.d.f. $g_0(r)$ and the equation of state Z_0 of the HS reference fluid, Henderson and coworkers^{22,23,24,25,26,27}, and many others, applied successfully the BH theory to a variety of model fluids.

The Barker-Henderson theory has been sometimes applied to crystalline solids.^{10,28,29,30} To apply this theory, accurate expressions for the compressibility factor Z_0 and the r.d.f. $g_0(r)$ of the hard-sphere reference fcc solid are needed. The equation of state of a fcc hard-sphere solid is well reproduced by the Hall³¹ equation

$$\begin{aligned} Z_0 = & 3/\alpha + 2.557696 + 0.1253077\beta + 0.1762393\beta^2 - 1.053308\beta^3 + 2.818621\beta^4 \\ & - 2.921934\beta^5 + 1.118413\beta^6 \end{aligned} \quad (27)$$

where $\beta = 4\alpha/(1 + \alpha)$ and $\alpha = \rho_0/\rho - 1$, in which ρ_0 is the close-packing density.

Regarding the radial distribution function of the fcc hard-sphere solid, accurate parametrizations are available.^{32,33,34,35} One of the most frequently used is³³

$$g_0(x) = \frac{A}{x} \exp \left[-W_1^2 (x - x_1)^2 - W_2^4 (x - x_1)^4 \right] + \frac{W}{24\eta\sqrt{\pi}} \sum_{i=2}^{\infty} \frac{n_i}{x_i x} \exp \left[-W^2 (x - x_i)^2 \right] \quad (28)$$

where $\eta = (\pi/6)\rho^*$ is the packing fraction and x_1 is the position of the first peak of the r.d.f., which was determined^{32,33} from the simulation data for several packing fractions. Functions W_1 , W_2 , and W are given by³⁶

For $\eta \leq 0.55$:

$$W_1 = \sqrt{3}W_2 = \frac{\sqrt{3}}{0.50552} \exp [10.49375 (\eta - 0.52)] \quad (29)$$

$$W = \frac{\sqrt{3}/2}{[0.23601 (\eta - \eta_0)^2 - 21.4395 (\eta - \eta_0)^5]^{1/2}} \quad (30)$$

For $0.55 < \eta \leq 0.73$:

$$W_1 = \frac{1.5522782}{\eta_0 - \eta} - 2.0302556 \exp [5.8331273 (\eta_0 - \eta)] + 74.873192 (\eta_0 - \eta)^2 \quad (31)$$

$$W_2 = \frac{0.9559565 - 5.855022 (\eta_0 - \eta) + 39.74663 (\eta_0 - \eta)^2 - 109.62638 (\eta_0 - \eta)^3}{\eta_0 - \eta} \quad (32)$$

$$W = \frac{1 - 10.589574 (\eta_0 - \eta)^{2.543}}{[0.694 (\eta_0 - \eta)]^{1.072}} \quad (33)$$

In the preceding expressions η_0 is the packing fraction corresponding to the close packing density ρ_0 for the fcc solid.

Finally, parameter A in expression (28) from the condition that the virial theorem

$$Z_0 = 1 + 4\eta g_0(1) \quad (34)$$

must be satisfied.

IV. RESULTS AND DISCUSSION

In Figure 1, the results for the excess energy from the BH and MC perturbation theories are compared with each other and with the MC simulation data listed in Tables I-IV, and a similar comparison is performed in Figure 2 for the compressibility factor. The upper limits in the integrals involved in the BH perturbation theory were set at $x = 3.0$, thus making possible a direct comparison with simulation data without need of including in the latter the corrections due to the truncation of the potential. Let us first examine the MC simulation data. At densities $\rho^* \lesssim 0.95$ all the systems studied underwent a melting transition. Moreover, at the lowest temperatures considered the transition showed a tendency, clearly seen in the figures, to displace towards higher densities ($\rho^* \approx 1.0$), and the effect is more pronounced the higher is the value of γ . This is a consequence of the clustering of the particles of these systems at low temperatures.

Regarding the MC-P results for the excess energy U^E , one can see in Figure 1 that this 'exact' first-order perturbation theory reproduces very accurately the simulation data for all the values of γ , at all temperatures and densities except near melting at low temperatures. The same is true for the compressibility factor Z , as shown in Figure 2, except for $\gamma \geq 12$ and $T^* = 0.6$, the lowest temperature considered, and perhaps sometimes for $T^* = 0.8$ too. The reason for the better performance of the MC-P results for the excess energy than for the compressibility factor is, at least partially, because this 'exact' perturbation theory is second order in the former quantity whereas it is only first order in the radial distribution function and the equation of state.

Now, let us analyze the performance of the BH perturbation theory. For the excess energy, at temperatures $T^* \geq 1.5$, the contribution of the second-order term is nearly negligible, so that the BH theory truncated at first order provides satisfactory results in all cases for $T^* \geq 1.5$ and even for lower temperatures in the case $\gamma = 6$. For $\gamma = 12$ and $T \leq 1.0$, second-order approximation is needed, with the local compressibility approximation providing grater accuracy than the macroscopic compressibility approximation. For $\gamma \geq 18$ and $T \leq 1.0$, the second-order approximation fails to provide completely satisfactory results for the low-density solid. It is to be remarked that even in the cases where the BH theory departs from simulation data, the 'exact' first-order MC-P continues doing a good job.

As far as the equation of state is concerned, Figure 2 shows that the BH perturbation

theory is in complete agreement with the MC-P theory up to densities close to the melting density, except perhaps for $\gamma \leq 18$ and $T^* = 0.6$, with little or no difference between first- and second-order approximations, although the local compressibility approximation seems to work slightly better at low temperatures than the first-order or the macroscopic compressibility approximations.

From the precedent analysis it seems clear that if we were able of improving the theoretical predictions for the excess energy until reaching the accuracy of the MC-P results, and using the Helmholtz free energy route to obtain the equation of state instead of the pressure equation, the results obtained from the perturbation theory would probably be in complete agreement with simulation data for solids with spherically symmetrical potentials even for extremely short-ranged potentials and low temperatures. While this improvement is achieved, the Barker-Henderson perturbation theory constitutes an excellent choice in most situations.

ACKNOWLEDGMENT

Financial support by the Spanish Ministerio de Ciencia y Tecnología (MCYT) under Grant No. BFM2003-001903 is acknowledged.

* Author to whom correspondence should be addressed; Electronic address: ramon.solana@unican.es

¹ Ben-Amotz, D.; Stell G. *J. Chem. Phys.* **2003**, *119*, 10777-10788.

² Coutinho, J. A. P.; Vlamos, P. M.; Kontogeorgis, G. M. *Ind. Eng. Chem. Res.* **2000**, *39*, 3076-3082.

³ Elvassore, N.; Prausnitz, J. M. *Fluid Phase Equil.* **2002**, *194-197*, 567-577.

⁴ Murakami, M. *J. Chem. Phys.* **2004**, *120*, 6751-6755.

⁵ Zhang, Q.; Archer, L. A. *J. Chem. Phys.* **2004**, *121*, 10814-10824.

⁶ Heyes, D. M.; Woodcock, L. V. *Mol. Phys.* **1986**, *59*, 1369-1388.

⁷ Díez, A.; Largo, J.; Solana, J. R. *J. of Chem. Phys.* **2006**, *125*, 074509-1-074509-12.

- ⁸ Díez, A.; Largo, J.; Solana, J. R. *Fluid Phase Equil.* In the press.
- ⁹ Camp, P. J.; Patey, G. N. *J. Chem. Phys.* **2001**, *114*, 399-408.
- ¹⁰ Camp, P. J. *Phys. Rev. E* **2003**, *67*, 011503-1-011503-8.
- ¹¹ Kurochkin, V. I. *Sov. Phys. Lebedev Inst. Rep (USA)* **1990**, *8* 1-2.
- ¹² Largo, J.; Solana, J. R. *Int. J. Thermophys.* **2000**, *21*, 899-908.
- ¹³ Jiuxun, S. *Can. J. Phys.* **2005**, *83* 55-66.
- ¹⁴ Barker, J. A.; Henderson, D. *J. Chem. Phys.* **1967**, *47*, 2856-2861.
- ¹⁵ Barker, J. A.; Henderson, D. *Ann. Rev. Phys. Chem.* **1972**, *23*, 439-484.
- ¹⁶ Tang, Y.; Lu, B.C.-Y. *J. Chem. Phys.* **1993**, *99*, 9828-9835.
- ¹⁷ Tang, Y.; Lu, B.C.-Y. *Mol. Phys.* **1997**, *90*, 215-224.
- ¹⁸ Smith, W. R.; Henderson, D.; Barker, J. A. *J. Chem. Phys.* **1971**, *55*, 4027-4033.
- ¹⁹ Largo, J.; Solana, J. R. *Mol. Simulat.* **2003**, *29*, 363-371.
- ²⁰ Largo, J.; Solana, J. R. *Fluid Phase Equil.* **2003**, *212*, 11-29.
- ²¹ Largo, J.; Solana, J. R. *J. Phys. Chem. B* **2004**, *108*, 10062-10070.
- ²² Barker, J. A.; Henderson, D. *J. Chem. Phys.* **1967**, *47*, 4714-4721.
- ²³ Barker, J. A.; Henderson, D. *4th Symp. Thermophys. Properties* **1968**, 30-36.
- ²⁴ Smith, W. R.; Henderson, D.; Barker, J. A. *Can. J. Phys.* **1968**, *46*, 1725-1727.
- ²⁵ Smith, W. R.; Henderson, D.; Barker, J. A. *J. Chem. Phys.* **1970**, *53*, 508-515.
- ²⁶ Smith, W. R.; Henderson, D.; Barker, J. A. *Can. J. Phys.* **1975**, *53*, 5-12.
- ²⁷ Henderson, D.; Scalise, O. H.; Smith, W. R. *J. Chem. Phys.* **1980**, *72*, 2431-2438.
- ²⁸ Tavares, F. W.; Sandler, S. I. *AIChE J.* **1997**, *43*, 219-231.
- ²⁹ Tavares, F. W.; Prausnitz, J. M. *Colloid Polym. Sci.* **2004**, *282*, 620-632.
- ³⁰ Zhou, S. *J. Phys. Chem. B* **2004**, *108*, 8447-8451.
- ³¹ Hall, K. R. *J. Chem. Phys.* **1972**, *57*, 2252-2254.
- ³² Weis, J.-J. *Mol. Phys.* **1974**, *28*, 187-195. Ibid. **1976**, *32*, 296.
- ³³ Kincaid, J. M.; Weis, J. J. *Mol. Phys.* **1977**, *34*, 931-938.
- ³⁴ Rascón, C.; Mederos, L.; Navascués, G. *J. Chem. Phys.* **1996**, *105*, 10527-10534.
- ³⁵ Velasco, E.; Mederos, L.; Navascués, G. *Mol. Phys.* **1999**, *97*, 1273-1277.
- ³⁶ Kang, H. S.; Ree, T.; Ree, F. H. *J. Chem. Phys.* **1986**, *84*, 4547-4557.

List of Tables

TABLE I: Simulation data for $\gamma = 6$. Corrections due to the truncation of the potential have not been included. The number between parenthesis indicates the error in the last significant digit of the compressibility factor. For the excess energy, the statistical error in most cases is beyond the third decimal place and when this is the case it is not indicated.

ρ^*	0.90	0.95	1.00	1.05	1.10	1.15	1.20	1.25	1.30
<hr/>									
$T^* = 0.6$									
Z	2.70(2)	3.75(3)	0.53(2)	0.28(2)	0.70(2)	1.66(2)	3.84(2)	8.05(3)	17.41(4)
$U^E/N\epsilon$	-3.382	-3.651	-3.852	-4.149	-4.479	-4.832	-5.208	-5.610	-6.036
$T^* = 0.8$									
Z	4.59(2)	5.96(3)	2.84(2)	3.04(2)	3.75(2)	5.22(2)	7.71(2)	12.42(3)	22.24(4)
$U^E/N\epsilon$	-3.351	-3.630	-3.835	-4.141	-4.473	-4.829	-5.207	-5.609	-6.036
$T^* = 1.0$									
Z	5.85(2)	7.22(2)	4.32(2)	4.72(2)	5.65(2)	7.29(2)	10.05(2)	15.01(3)	25.04(4)
$U^E/N\epsilon$	-3.336	-3.616	-3.826	-4.136	-4.470	-4.827	-5.206	-5.609	-6.036
$T^* = 1.5$									
Z	7.481(2)	9.04(2)	6.23(2)	6.95(2)	8.16(2)	10.07(2)	13.15(2)	18.49(2)	28.91(4)
$U^E/N\epsilon$	-3.319	-3.602	-3.815	-4.129	-4.466	-4.825	-5.205	-5.609	-6.036
$T^* = 2.0$									
Z	8.277(2)	9.77(6)	7.24(2)	8.06(2)	9.41(2)	11.50(2)	14.73(2)	20.21(2)	30.79(4)
$U^E/N\epsilon$	-3.310	-3.593(1)	-3.810	-4.126	-4.464	-4.824	-5.204	-5.609	-6.036
$T^* = 3.0$									
Z	9.12(2)	8.18(4)	8.23(1)	9.21(2)	10.74(2)	12.92(2)	16.29(2)	21.92(2)	32.71(4)
$U^E/N\epsilon$	-3.303	-3.529(1)	-3.805	-4.123	-4.463	-4.823	-5.204	-5.608	-6.036

TABLE II: As in Table I for $\gamma = 12$.

ρ^*	0.90	0.95	1.00	1.05	1.10	1.15	1.20	1.25	1.30
<hr/>									
$T^*=0.6$									
Z	4.54(3)	5.61(3)	5.98(9)	2.52(2)	2.03(3)	1.86(3)	2.36(3)	4.43(3)	10.884(4)
$U^E/N\epsilon$	-2.018(1)	-2.221(1)	-2.432(2)	-2.510	-2.760	-3.068	-3.442	-3.892	-4.429
$T^*=0.8$									
Z	6.06(2)	7.44(3)	5.03(3)	4.61(2)	4.68(2)	5.21(2)	6.54(3)	9.64(3)	17.28(4)
$U^E/N\epsilon$	-1.951(1)	-2.167(1)	-2.247(1)	-2.458	-2.724	-3.046	-3.430	-3.886	-4.428
$T^*=1.0$									
Z	7.04(2)	8.36(3)	5.87(2)	5.97(2)	6.40(2)	7.31(2)	9.13(3)	12.77(3)	21.195(4)
$U^E/N\epsilon$	-1.919(1)	-2.130(1)	-2.205(1)	-2.431	-2.707	-3.035	-3.423	-3.883	-4.427
$T^*=1.5$									
Z	8.26(2)	9.88(2)	7.23(2)	7.66(2)	8.61(2)	10.09(2)	12.49(2)	16.96(3)	26.23(4)
$U^E/N\epsilon$	-1.873(1)	-2.089	-2.159	-2.396	-2.683	-3.019	-3.414	-3.880	-4.426
$T^*=2.0$									
Z	8.86(2)	10.59(2)	7.96(2)	8.60(2)	9.72(2)	11.49(2)	14.17(2)	19.10(3)	28.76(4)
$U^E/N\epsilon$	-1.851	-2.070	-2.139	-2.381	-2.671	-3.011	-3.409	-3.878	-4.426
$T^*=3.0$									
Z	9.46(2)	10.5(1)	8.71(2)	9.53(2)	10.95(2)	12.89(2)	15.93(2)	21.18(3)	31.36(4)
$U^E/N\epsilon$	-1.829	-2.014	-2.119	-2.366	-2.661	-3.004	-3.406	-3.876	-4.425

TABLE III: As in Table I for $\gamma = 18$.

ρ^*	0.90	0.95	1.00	1.05	1.10	1.15	1.20	1.25	1.30
<hr/>									
<u>$T^* = 0.6$</u>									
Z	5.411(3)	6.40(3)	6.83(7)	4.17(3)	3.48(4)	3.02(3)	2.68(3)	2.89(4)	6.48(5)
$U^E/N\epsilon$	-1.604(1)	-1.778(2)	-1.945(3)	-1.995(2)	-2.191(1)	-2.454(1)	-2.790	-3.231	-3.822
 <u>$T^* = 0.8$</u>									
Z	6.73(2)	8.04(3)	6.81(3)	5.80(2)	5.77(3)	5.95(3)	6.65(3)	8.43(4)	13.85(6)
$U^E/N\epsilon$	-1.511(1)	-1.695(1)	-1.778(2)	-1.898(1)	-2.116(1)	-2.396	-2.754	-3.214	-3.817
 <u>$T^* = 1.0$</u>									
Z	7.58(2)	8.96(2)	6.81(3)	6.88(2)	7.20(3)	7.85(3)	9.09(3)	11.74(4)	18.23(4)
$U^E/N\epsilon$	-1.465(1)	-1.647(1)	-1.673(1)	-1.849(1)	-2.078	-2.368	-2.734	-3.204	-3.813
 <u>$T^* = 1.5$</u>									
Z	8.63(2)	10.25(2)	7.96(2)	8.33(2)	9.15(2)	10.42(2)	12.45(3)	16.23(3)	24.36(4)
$U^E/N\epsilon$	-1.402(1)	-1.587(1)	-1.603(1)	-1.787	-2.029	-2.331	-2.710	-3.191	-3.809
 <u>$T^* = 2.0$</u>									
Z	9.22(2)	10.82(2)	8.46(2)	9.11(2)	10.20(2)	11.71(2)	14.16(2)	18.51(3)	27.37(3)
$U^E/N\epsilon$	-1.376(1)	-1.558	-1.565(1)	-1.759	-2.006	-2.313	-2.698	-3.186	-3.807
 <u>$T^* = 3.0$</u>									
Z	9.73(2)	11.58(2)	9.03(2)	9.86(2)	11.20(2)	13.09(2)	15.89(2)	20.77(3)	30.41(3)
$U^E/N\epsilon$	-1.347(1)	-1.536	-1.533	-1.732	-1.984	-2.297	-2.687	-3.180	-3.805

TABLE IV: As in Table I for $\gamma = 36$.

ρ^*	0.90	0.95	1.00	1.05	1.10	1.15	1.20	1.25	1.30
<hr/>									
$T^* = 0.6$									
Z	6.17(2)	7.20(2)	7.24(6)	5.95(3)	5.86(3)	5.79(3)	5.47(3)	4.88(4)	4.11(6)
$U^E/N\epsilon$	-1.061(2)	-1.194(1)	-1.284(5)	-1.319(2)	-1.460(2)	-1.648(2)	-1.890(1)	-2.233(1)	-2.753
$T^* = 0.8$									
Z	7.58(2)	8.89(3)	7.72(4)	7.61(3)	8.00(3)	8.47(3)	9.03(3)	9.91(5)	12.05(6)
$U^E/N\epsilon$	-0.960(1)	-1.097(1)	-1.100(2)	-1.192(2)	-1.341(1)	-1.536(1)	-1.794(1)	-2.160	-2.716
$T^* = 1.0$									
Z	8.42(2)	9.80(2)	8.11(2)	8.53(2)	9.07(3)	9.95(3)	11.07(3)	12.92(4)	16.78(6)
$U^E/N\epsilon$	-0.907(1)	-1.033(1)	-1.012(1)	-1.126(1)	-1.272(1)	-1.471(1)	-1.739(1)	-2.119	-2.695
$T^* = 1.5$									
Z	9.32(2)	11.02(3)	8.81(2)	9.49(2)	10.54(2)	11.90(2)	13.89(3)	16.97(4)	23.19(4)
$U^E/N\epsilon$	-0.838(1)	-0.970(1)	-0.919(1)	-1.034(1)	-1.188	-1.393	-1.673	-2.070	-2.669
$T^* = 2.0$									
Z	9.65(2)	11.45(2)	9.22(2)	10.01(2)	11.21(2)	12.85(3)	15.28(2)	19.09(3)	26.46(4)
$U^E/N\epsilon$	-0.802	-0.930(1)	-0.877(1)	-0.992	-1.149	-1.357	-1.642	-2.047	-2.657
$T^* = 3.0$									
Z	10.03(2)	11.59(6)	9.56(2)	10.51(2)	11.89(2)	13.82(2)	16.66(2)	21.19(3)	29.87(4)
$U^E/N\epsilon$	-0.771	-0.883(3)	-0.838	-0.954	-1.112	-1.321	-1.611	-2.026	-2.647

List of Figures

FIG. 1: Comparison between MC simulations (filled circles) and perturbation theory for the excess energy $U^E/N\epsilon$ of Sutherland solids for $T^* = 0.6, 0.8, 1.0, 1.5, 2.0$, and 3.0 from the bottom upwards. Open circles are the results from the MC perturbation theory as obtained from eq. (20). MC and MC-P results are indistinguishable at the scale of the figure in most cases. Dotted curves are the results from the first-order Barker-Henderson perturbation theory. Dashed and continuous curves are the results from the second-order Barker-Henderson perturbation theory using the macroscopic and local compressibility approximations, respectively. In most cases, the three curves are nearly indistinguishable to each other at the scale of the figure. For each temperature the curves, and the corresponding sets of data, have been displaced upwards for clarity by 1 unit with respect to those corresponding to the temperature immediately below.

FIG. 2: Comparison between MC simulations (filled circles) and perturbation theory for the compressibility factor $Z = pV/Nk_B T$ of Sutherland solids for $T^* = 0.6, 0.8, 1.0, 1.5, 2.0$, and 3.0 from the bottom upwards. Open circles are the results from the MC perturbation theory as obtained from eq. (21). Again, MC and MC-P results are nearly indistinguishable to each other. The curves have the same meaning as in fig. 1. For each temperature the curves, and the corresponding sets of data, have been displaced upwards for clarity by 5 units with respect to those corresponding to the temperature immediately below.

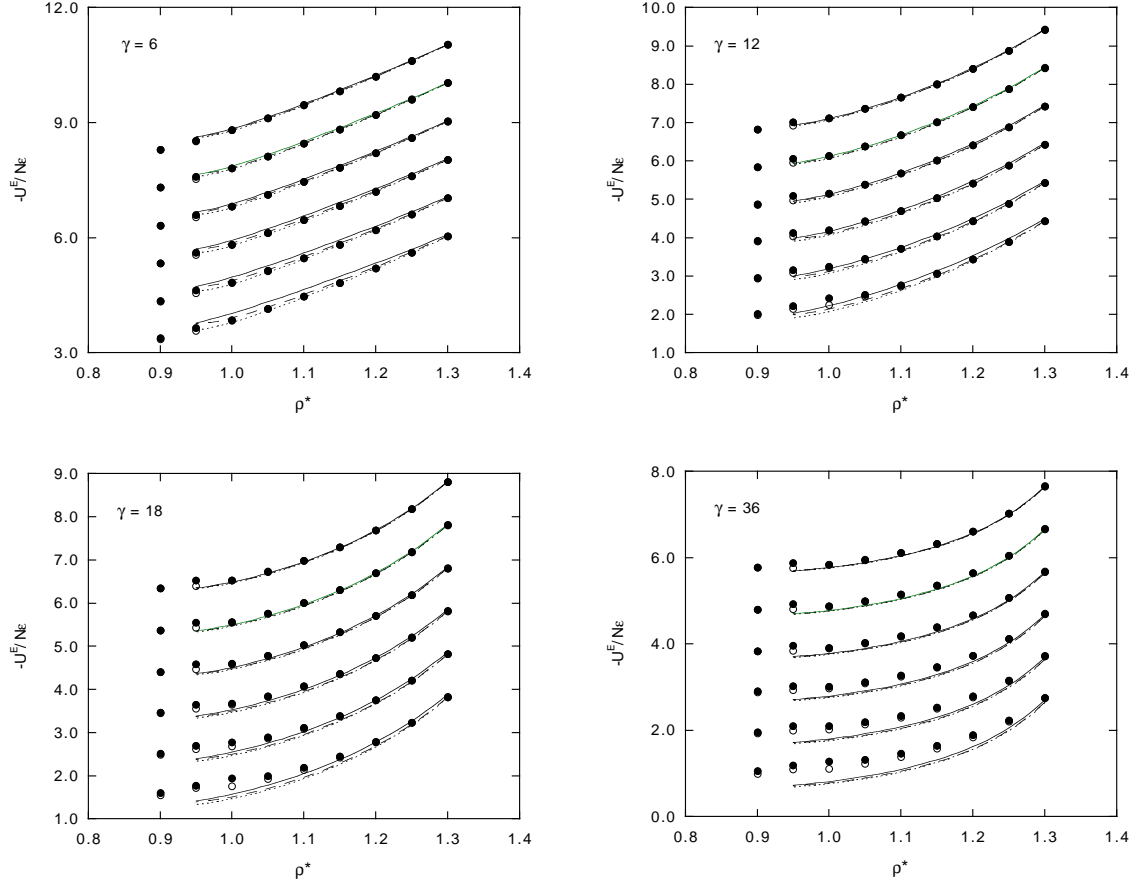


FIG. 1:

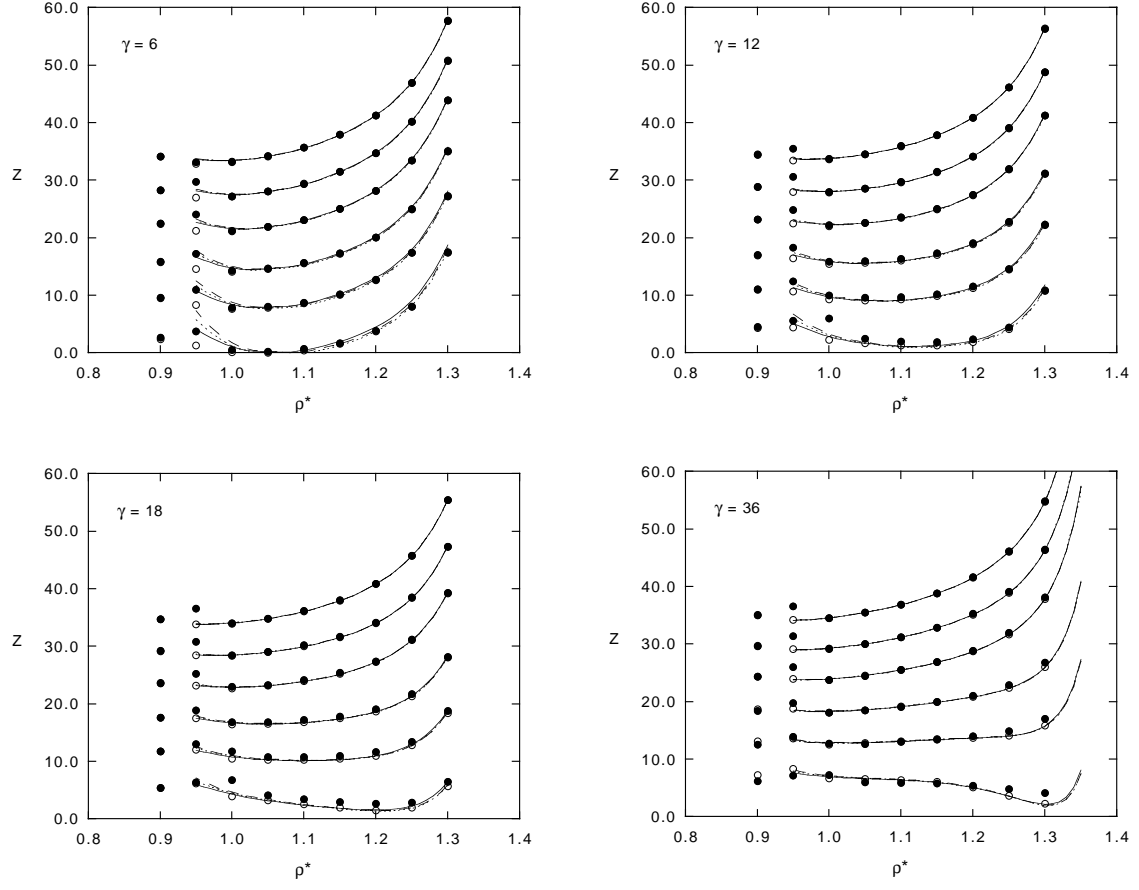


FIG. 2: